Seismic response of RC frames with steel-concrete truss beams equipped with beam-to-column and column-to-foundation friction damper connections

Seismic response of RC frames with steel-concrete truss beams equipped with beam-to-column and column-to-foundation friction damper connections

Risposta sismica di telai in c.a. con travi in acciaio-calcestruzzo reticolari dotati di connessioni travi-colonna e colonna-fondazione dissipative per attrito

Piero Colajanni[1], Lidia La Mendola[1], Alessia Monaco[2], Salvatore Pagnotta[1]

[1] *Department of Engineering, University of Palermo, Palermo, Italy*

[2] *Department of Architecture and Design, Politecnico di Torino, Torino, Italy*

ABSTRACT: Friction Damper Devices (FDDs) at the Beam-to-Column Connections (BCCs) are a suitable solution to prevent losses of performance due to cracking and bond losses caused by the high percentage of reinforcement that characterize the panel zone of Moment Resistant Frames with Hybrid Steel Trussed-Concrete Beams (HSTCBs). Here it will be shown that excellent seismic performance can be obtained only when FDDs at the BCCs are used in conjunction with self-centering dissipative connections at the column bases. To this aim, comparison of the seismic performance of traditional and innovative RC structures built using HSTCBs is performed, focusing on the different level of damage experienced by RC beams, columns and panel node zones belonging to traditional and innovative frames./ Nei telai in c.a. con travi Prefabbricate REticolari Miste (PREM) l'impiego di connessioni trave-colonna dissipative per attrito è una efficace soluzione per prevenire la perdita di prestazioni dovuta all'ampia fessurazione del nodo e alla perdita di aderenza delle barre di armature causata dall'elevata percentuale e dai grandi diametri utilizzati. In questo lavoro verrà mostrato che eccellenti prestazioni sismiche possono essere ottenute solo quando la connessione trave-colonna dissipativa viene impiegata insieme a connessioni ricentranti dissipative alla base della colonna. A tale scopo, vengono confrontate le risposte sismiche di telai con travi PREM tradizionali e con connessioni dissipative, evidenziando il diverso livello di danneggiamento subito dalle travi, dalle colonne e dal pannello di nodo di telai tradizionali e telai dotati di dispositivi dissipativi.

KEYWORDS: friction dampers, hybrid steel-trussed concrete beams, cyclic behavior of beam-column joints, self-centering systems, low-damage structures

1 INTRODUCTION

In the last years, the partial prefabrication of the construction process of RC frames takes advantage from the use of Hybrid Steel Trussed Concrete beams (HSTCBs). Nevertheless, in seismic areas, some issues arise due to the damage of the beam-to-column panel zone where usually a very large amount of longitudinal reinforcement is present and, consequently, the possibility of introducing the adequate amount of stirrups is limited.

In such cases, energy-dissipating devices at the beam-column connection can be adopted in order to absorb the seismic energy, preventing the damage of the structural elements and limiting the economic impact due to the structural repair after catastrophic events. Furthermore, if devices endowed of increased lever arm of the bending moment are used, the shear forces acting on the joint panel can be reduced and its damage can be prevented.

This paper presents an innovative solution for Beam-to-Column Connections (BCCs) to be adopted for cast-in-situ RC frames in the presence of HSTCBs, as proposed by Colajanni et al. (2020, 2021). The considered HSTCB is made of a steel truss with diagonal V-shaped rebars welded on the top to a variable number of bars constituting the upper chord and on the bottom to a steel plate usually employed in constructional steelwork (Colajanni et al. 2016, Colajanni et al. 2018a, 2018b;).

In order to allow the RC members working in an almost elastic field, they need to be overstrengthened. This achievement is hindered by the uncertainties that affect the friction devices because of the variability of the bolt preload and the value of the friction coefficient between the sliding surfaces (Ferrante Cavallaro et al. 2018). This paper shows how the use of Friction Damper Device (FDD) at the BCC in RC frames with HSTCBs is an appropriate solution for preventing the decrease of mechanical performance within the panel zone; moreover, the presented research shows that the use of self-centering dissipative connections at the column bases is an effective tool for achieving excellent seismic performance.

Three different configurations of frames are investigated: i) Innovative Frame (IF), equipped with FDDs at the BCCs; ii) Innovative Frame with Threaded

Bars (IF-TB), with FDDs provided with preloaded threaded bars and disk springs at the Column-to-Foundation Connection (CFC); iii) Innovative Frame with Friction Devices (IF-FD), which, in addition to FDDs at the BCCs, is equipped with a self-centering friction connection at the CFC readapted from that proposed for steel frames by Latour et al. (2019).

Non-Linear Time History Analyses (NLTHAs) are performed in order to compare the seismic response of the IFs with the behaviour of the Traditional Frames (TF) without friction dampers. Finally, the Park & Ang Index (Park & Ang 1985) is used to calculate the different amount of damage in the RC members of the four frames.

2 CYCLIC RESPONSE OF RC BEAM-COLUMN JOINTS

For the modelling of the cyclic behavior of beam-column joints of RC frames with HSTCBs, the results of an experimental campaign previously carried out by some of the Authors are taken into account (Colajanni et al. 2016). The subassemblies tested were representative of four-way beam-column joints, constituted as follows: two half-columns with cross-section 300 × 400 mm, reinforced with ten 20 mm diameter rebars; two HSTCBs with 5-mm thick lower steel plate, 3ϕ16 longitudinal upper rebars and ϕ12 diagonal rebars at 300 mm spacing. The beam cross-section is equal to 300 × 250 mm. The bending moment resistance of the beam end section is obtained neglecting the truss contribution and considering only the added top and bottom longitudinal reinforcement, namely 4ϕ24 and 2ϕ24 bars, respectively.

Degrading strength and stiffness were observed as well as the pinching of hysteretic cycles. In this paper, aiming at calibrating the cyclic behavior of the joint, the results of one of the tested subassemblies are used, namely those of the specimen subjected to an axial force of 800 kN in the column.

2.1 *Fundamentals of the mechanical modelling*

The degrading phenomena of the joint are taken into account by means of the mechanical model proposed by Lowes and Altoontash (2003). This model is depicted in Figure 1. A four-node, 12 DOFs super-element is used, which includes a 2D shear element, representing the concrete core of the joint, connected to eight linear springs aimed at reproducing the strength and stiffness degradation caused by slippage of the longitudinal reinforcement, and four linear springs able to reproduce the actual interface shear behavior affected by crack openings. Several simplified assumption are introduced for the definition of the anchorage behavior: - the bond stress throughout the anchorage-zone of the longitudinal reinforcement is assumed constant if the bar is loaded below the

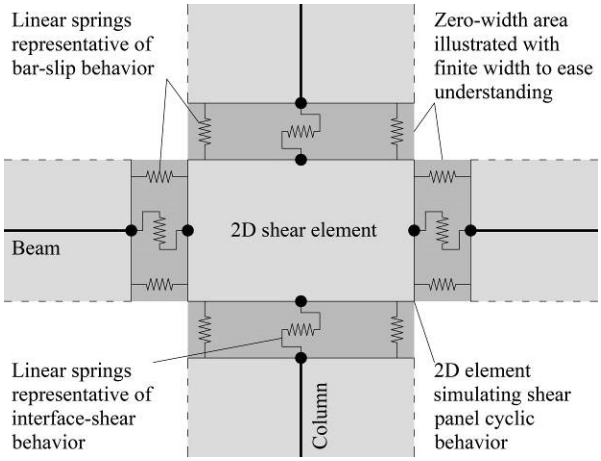

Figure 1. RC beam-column joint model / Modello del nodo trave-colonna.

elastic limit, or piecewise constant for bars experiencing yielding; the bar slip determines the relative displacement between the bar and concrete core perimeter and it is related to the strain state experienced by the bar; no slip is assumed at the section of zero normal stresses. Finally, the equations linking the bar–stress (f_s) and bar–slip (s) are the following:

$$s = \frac{d_b f_s^2}{8E\tau_E} \qquad f_s \le f_y$$
$$s = \frac{d_b}{4}\left\{\frac{f_y^2}{2E\tau_E} + \frac{f_s - f_y}{\tau_Y}\left[\frac{f_y}{E} + \frac{\left(f_s - f_y\right)}{2E_h}\right]\right\} \qquad f_s > f_y \tag{1}$$

where E is the elastic modulus of steel; E_h the strain hardening modulus; d_b the nominal rebar diameter; f_s the bar stress at the concrete core perimeter; f_y the steel yield stress; τ_E the bond stress in case of elastic steel; τ_Y the bond stress in case of yielded steel; A_b cross-sectional area of rebar.

2.2 *Results and validation*

The FE software SeismoStruct is used for simulating the joint behavior by implementing the macro model described before. Firstly, the model of the benchmark test on the subassembly is generated and then the behavior of both traditional and innovative frames is reproduced.

In the FE model, 2D shear-panel components and 3D bar-slip linear springs are implemented by means of link elements, featured by uncoupled axial, shear and flexural behavior. Figure 2 depicts the scheme of the structural model employed to adapt the aforementioned beam-column joint model into the FE software used for the simulations: - one rotational spring at the center of the joint simulates the relative rotation between columns and beams due to the shear deformation of the joint; four other rotational springs are used for modeling the relative rotation of beams and columns due to slippage of the longitudinal bars within the concrete core. Finally, four rigid

links within the panel zone are used for assuming that the behavior of the central rotational spring completely rules the cyclic behavior of the joint.

The parameters adopted for the modelling of the rotational spring are shown in Table 1 and Table 2, respectively for the panel zone and the bar-slip mechanism. Regarding panel zone, parameters defining the backbone curve are calculated by means of Modified Compression Field Theory (MCFT), while for those describing cyclic behavior are used the values suggested by Sivaselvan and Reinhorn (1999). Concerning bar-slip mechanism, parameters governing backbone curve are computed as suggested in previous section, while those defining cyclic behavior are tuned on the basis of the experimental results.

Figure 3 shows the comparison between experimental and numerical curves of the subassembly with and without damage of the panel zone (i.e. by modeling or not the above-mentioned degrading phenomena affecting cyclic response of joints), proving that the model is capable of reproducing the degrading of both stiffness and strength as well as the pinching of the hysteretic cycles.

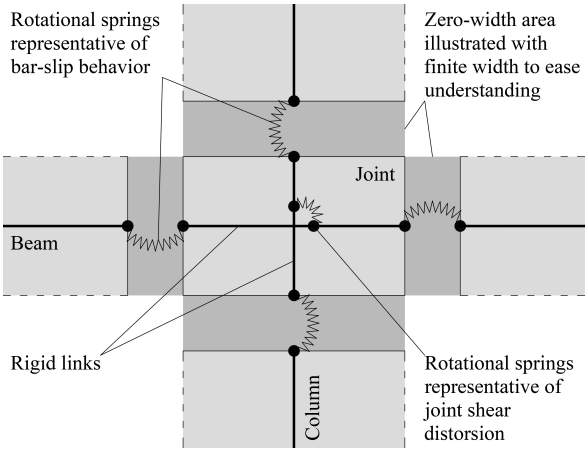

Figure 2. Structural model implemented in SeismoStruct / Modello strutturale implementato in SeismoStruct.

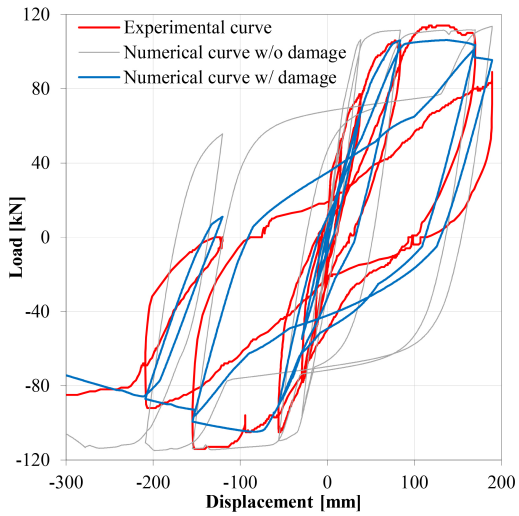

Figure 3. Experimental and numerical curves of the subassembly with and without damage of the panel zone / Curve numeriche e sperimentali del sub-assemblaggio con e senza danneggiamento del pannello di nodo.

Table 1. Parameters of the rotational spring element for modeling the cyclic behavior of the Panel Zone in the Subassembly (PZ-S), Traditional Frame (PZ-TF) and Innovative one (PZ-IF) / Parametri della molla rotazionale per la modellazione del comportamento ciclico del pannello di nodo del sub-assemblaggio (PZ-S), del telaio tradizionale (PZ-TF) e del telaio innovativo (PZ-IF).

	PZ-S	PZ-TF	PZ-IF
First-class parameters (backbone curve)			
Initial rotational stiffness (kNm/rad)	235000	245000	330000
Cracking moment (kNm)	47	49	66
Yield moment (kNm)	290	298	406
Yield rotation (rad)	0.006	0.006	0.006
Ultimate rotation (rad)	0.2	0.2	0.2
Post-yield stiffness ratio as % of elastic	0.001	0.001	0.001
Second-class parameters (hysteresis shape)			
Stiffness degradation	4	4	4
Ductility based strength decay	0.6	0.6	0.6
Hysteretic energy based strength decay	0.6	0.6	0.6
Slip parameter	0.5	0.5	0.5

Table 2. Parameters of the rotational spring element for modeling the cyclic behavior of the Bar-Slip mechanism in the Subassembly (BS-S) and Traditional Frame (BS-TF) / Parametri della molla rotazionale per la modellazione del comportamento ciclico del meccanismo di scorrimento delle barre nel sub-assem-blaggio (PZ-S) e nel telaio tradizionale (PZ-TF).

	BS-S	BS-TF
First-class parameters (backbone curve)		
Elastic stiffness (kNm/rad)	52000	65000
Yield moment (kNm)	168/-94	174/-169
Rotation at peak moment strength (rad)	0.02/-0.02	0.02/-0.02
Peak moment strength (kNm)	176/-96	184/-179
Residual moment strength (kNm)	1.74/-0.93	1.86/-1.73
Second-class parameters (hysteresis shape)		
Pinching factor	0.5	0.5
Deterioration factor	0.6	0.6

3 FRICTION DEVICE AND SELF-CENTERING SYSTEMS

A thorough analysis of the FDD developed for HSTCBs can be found in Colajanni et al. (2020, 2021). The dissipative BCC showed in Figure 4 is constituted by a vertical central steel plate with curved slotted holes and steel angles on the lower part of the beam; high strength bolts are properly preloaded according to the slip force required. An upper T-stub is anchored to the column and bolted to a C- shaped steel profile, the latter welded to the upper longitudinal rebars of the steel truss of the HSTCB. When the slip friction force is reached, the dissipative system rotates around a point placed at the base of the T-stub, where the cross section is properly reduced. Rebars with variable inclination welded between the steel plate and the upper chord of the beam, are used for enhancing the stiffness between vertical central plate, steel truss top chord and concrete material.

As reported in Colajanni et al. (2020, 2021), the cyclic response of the beam endowed with BCC device calculated by means of FE simulations exhibits a symmetric response for a hogging and sagging bending moment and does not give rise to any damage in the loading-unloading phases.

For making earthquake-resilient structures, frames need to be endowed with self-centering systems able to keep the residual drift within a maximum allowable limit (e.g. 0.5 %). For this reason, two different self-centering solutions are herein proposed. The first consists of a column splice with cover plates on both flanges and web, with slotted holes on the column to ensure the rotation of the connection (Figure 5). Threaded bars and disk springs provide this CFC with an elastic bilinear moment-rotation response, avoiding formation of a plastic hinge at the column base. However, the connection has no dissipative capacity.

The FE analyses showed that this solution is not enough efficient to ensure limited maximum and residual interstory drifts. Thus, a second solution is further proposed by means of an adaptation of the one reported in Latour et al. (2019) for steel frames.

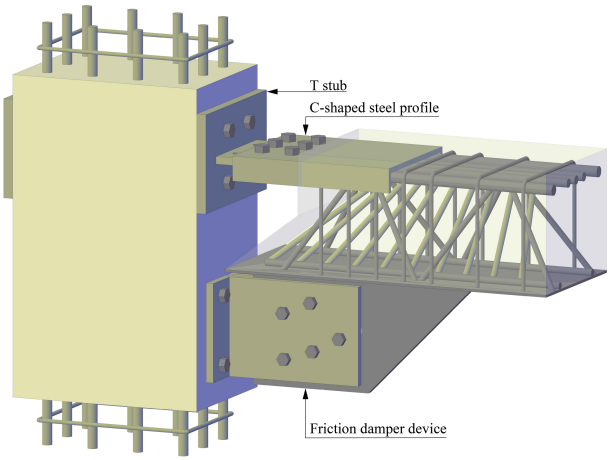

Figure 4. Structural solution adopted for the BCC / Soluzione adottata per la connessione trave-pilastro.

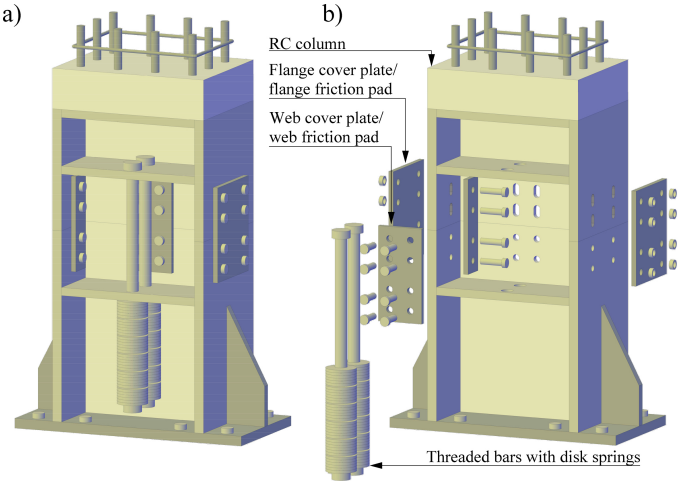

Figure 5. Self-centering connections at RC column base (a), exploded 3D view (b) / Connessione ricentrante alla base del pilastro (a), esploso di vista 3D (b).

In particular, in this paper the device is adapted to a RC column and the bearing type connections are substituted by friction pads with preloaded bolts, which ensure the adequate dissipative capacity.

4 RC FRAME AND SEISMIC INPUT

The FE model is generated for a two stories (3 m high) - two spans (5 m) RC frame, whose details are those reported in Section 2. The tributary seismic area leads to a distributed mass of 3.8 ton/m added on each story, in addition to the dead load.

Four types of frame are considered: the Traditional Frame (TF), the Innovative Frame with FDDs at the BCCs (IF), the Innovative Frame + unbounded Threaded Bars (i.e. post-tensioned tendons) as self-centering system (IF-TB), and the Innovative Frame + the adapted system employed in steel structures constituted by preloaded threaded bars, disk springs and Friction Devices (IF-FD). Thirty spectrum-compatible artificial accelerograms are used for modeling the seismic input. The target spectrum is that proposed by NTC 2008 for Reggio Calabria (Italy). The behavior factor q selected is 3.

4.1 *Innovative Frame model (IF)*

Figure 6 shows the node modeling scheme for RC frame with friction device used in the FE software.

The panel zone is modeled as in Figure 2, with a non-linear rotational spring representative of joint shear deformation, whose parameters are reported in Table 1. The friction device is represented by means of a bilinear kinematic rotational spring, whose parameters are: initial rotational stiffness 10^6 kN/rad, yield moment 110 kNm, post-yield stiffness ratio 10^{-4} as % of elastic one, defined in order to simulate rigid behavior in the elastic branch and with a very small stiffness in the post-yielding branch.

4.2 *Innovative Frame model with self-centering Friction Device (IF-FD)*

Non-linear rotational spring employing the Self Centering Brace (SCB) constitutive law is used for modelling the self-centering friction connection of the column bases of the IF-FD. Their design is developed according to the procedure reported in Latour et al. (2019). The design moment strength of the connection M_d^{FD} was set equal to 200 kNm (i.e. 75% of the bending moment resistance of the column). The self-centering behavior is ensured by the moment resistance value provided by the threaded bars and the axial force (decompression moment M_0) which is greater than that provided by the friction pads, M_1. Therefore, M_0 is set to 60% of the total moment resistance value (120 kNm). The design shear resistance value V_d^{FD} is equal to $2\Omega\, M_d^{FD} / L$ = 200 kN, where Ω=1.5 is the overstrength factor, and

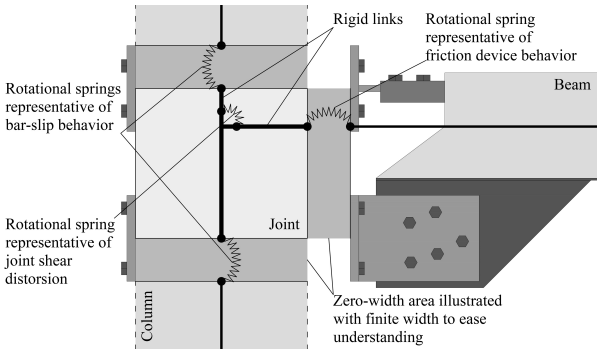

Figure 6. Node modeling scheme for RC frame with friction device / Modello di nodo per telai in c.a. con dispositivi ad attrito.

L=3 m is the column height. The shear force is demanded to the web friction pads: they consist in four M16 bolts of 10.9 class placed on each side, and two friction interfaces. To reduce the preload loss, the clamping force is limited in the range 30-60% of the clamping force calculated as suggested by EN 1993:1-8 (Ferrante Cavallaro et al. 2018). Thus, the ratio between the effective and maximum clamping force acting on the bolts of the web friction pads is:

$$r_w = \frac{V_d^{FD}}{\mu n_{ws} n_{wb} F_p} = 0.57 \tag{2}$$

where μ=0.4 is the friction coefficient, n_{ws} and n_{wb} are the number of friction interfaces and bolts, and F_p=110 kN is the clamping force. The moment strength provided by the web friction pads is:

$$M_{1,w} = r_w \mu n_{ws} n_{wb} F_p \frac{h}{2} = 40\,kNm \tag{3}$$

where $h/2$ is the approximated value assumed for the lever arm of the friction force. The moment capacity provided by both flange and web friction pads being M_1 = 80 kNm, the contribution due to the flange friction pads is thus $M_{1,f}$ = 40 kNm. The ratio between the effective and maximum clamping force is:

$$r_f = \frac{M_{1,f}}{\mu n_{fs} n_{fb} F_p h} = 0.29 \tag{4}$$

where n_{fs} is the number of interfaces and n_{fb} the number of bolts in the flange. The moment strength referred to the threaded bars $M_{0,tb}$ is the difference between the decompression moment M_0 and the bending moment in the column, $M_{0,af}$, associated to the axial force. For the lateral column N_l = 200 kN; thus, if $h/2$ is approximatively the lever arm of the axial force, then the values of $M_{0,af}$ = 40 kNm and $M_{0,tb}$ = 80 kNm are found. So, by using four M30 threaded bars class 10.9, the ratio between effective and maximum preload force is:

$$r_{tb} = \frac{M_0 - M_{0,af}}{n_{tb} F_{tb} h / 2} = 0.26 \tag{5}$$

where n_{tb} is the number of bars and F_{tb} = 393 kN the maximum preloading force. Hence, the effective preload force is $F_{t,eff} = r_{tb} F_{tb}$ = 100 kN.

In order to guarantee the elastic behavior of the threaded bars, disk springs has to be designed and coupled to the bars. The ultimate rotation of the system (θ_u = 40 mrad) induces a gap-opening Δ equal to 8 mm. Standard disk springs are chosen whose features are: internal diameter 31 mm, external diameter 76 mm, overall height 8.3 mm and thickness 6.6 mm. Their stiffness is about 60 kN/mm. Twelve groups in series of three disk springs in parallel have to be used for each bar, reaching a global stiffness K_{ds} of the disk springs of 15 kN/mm.

Finally, the stiffness of the branch after the attainment of M_d^{FD} is calculated for the definition of the moment-rotation response of the connection. Therefore, the stiffness of the threaded bar is calculated:

$$K_{tb} = \frac{E_{tb} A_{tb}}{l_{tb}} = 214\,kN/mm \tag{6}$$

Then, the rotational stiffness of the connection considering the stiffness contribution of both threaded bars and disk springs is given as:

$$K_{\theta,2}^{FD} = \frac{1}{\frac{4}{h^2}\left(\frac{1}{n_{tb}K_{tb}} + \frac{1}{n_{tb}K_{ds}}\right)} = 2261\,kNm/rad \tag{7}$$

Finally, the bending moment at the ultimate rotation is M_u^{FD} = 290 kNm.

Aiming at preventing the formation of a plastic hinge at the column base up to the ultimate rotation, 2ϕ20 are added to the column for enhancing the moment strength along its strong-axis direction.

The parameters of the SCB constitutive law used for the rotational spring elements adopted for the simulation of this connection are: initial rotational stiffness $K_{\theta,1}$=10^6 kNm/rad, yield moment=120 kNm, post-yeld stiffness $K_{\theta,2}$=2261 kNm/rad, ratio of forward to reverse yield moment equal to 10^{-4}.

4.3 *Innovative Frame model with preloaded threaded bars (IF-TB)*

The parameters used for characterizing the connection are those presented for IF-FD with the exception of the contribution to the moment strength provided by the friction devices because in IF-TB they are substituted by bearing type connections with un-preloaded bolts. Therefore, the design moment strength of the connection M_d^{TB} is equal to 120 kNm, given by the preload of the threaded bars and the axial force on the column. The stiffness of the post-yielding branch is $K_{\theta,2}^{FD}$, and therefore the ultimate moment strength M_u^{TB} results 210 kNm.

5 ANALYSIS OF RESULTS

The behavior of the four types of frames is compared carrying out NLTHAs which allows to analyze several parameters such as: mean and CoV of Maximum Interstory Drift Ratios (MIDRs) and Residual Interstory Drift Ratios (RIDRs); moment-rotation curves of beam end sections, column-base sections, link elements representing panel zone, bar-slip mechanism, friction device and self-centering systems. Furthermore, the Park & Ang damage Index (PAI) is calculated for the principal elements, which experience cyclic actions. Table 3 summarizes the average and CoV of MIDRs and RIDRs of the four types of RC frames.

It can be observed that TF and IF experience similar average values of MIDRs; however, the average RIDRs obtained in the IF is 300%-400% than those provided by the TF.

The introduction of self-centering system with a much lower yield moment in the IF-TB, leads to the increment of the average MIDR. However, the efficiency of the self-centering system is demonstrated by the RIDR average values significantly lower if compared to those of the IF.

The results obtained with the IF-TB show an unsatisfying behavior, with a reduction of the RIDR average value at the first floor and its increase at the second floor.

Among those explored, the most satisfactory behavior is exhibited by the IF-FD, which gives the lowest mean values of MIDRs and mean values of RIDRs similar to those of the TF. Actually, only one of the RIDR values is greater than the permissible value of 0.5 %. This result proves that the combination of innovative systems both at the BCC and CFC, with yielding strength lower than the strength of the connected members, is able to limit MIDR and RIDR.

Moreover, it is noteworthy to remark the role of friction devices and self-centering systems in the mitigation of the structural damage. To do so, the hysteresis cycles of dissipative elements for one accelerogram are compared, reporting the moment-rotation curves of the following elements:

- right end of the first-story second-span beam (Figure 7a for TF, Figure 7b for IF);
- link element representing the beam-column joint shear distortion of the first-story internal joint (Figure 7c for TF, Figure 7d for IF);
- link element connected to the right end of the aforementioned beam representing the bar-slip mechanism, for TF (Figure 7e);
- link element connected to the right end of the aforementioned beam representing the friction device, for IF (Figure 7f);
- link element connected to the base of the central column representing: the preloaded threaded bars and disk springs (in case of IF-TB) (Figure 7a2); the self-centering friction connection used in steel structures (in case of IF-FD) (Figure 7b2);
- base of the first-story central column (Figure 7c2 for TF, Figure 7d2 for IF, Figure 7e2 for IF-TB, Figure 7f2 for IF-FD).

The investigated beam end of the TF (Figure 7a) was subjected to slight plastic deformations due to the yielding of the bottom longitudinal reinforcement. Conversely, the investigated beam end of the IF (Figure 7b) exhibited an elastic behavior.

Observing the response of the link elements used for simulating the cyclic behavior of the beam-to-column joint, it can be noted that the panel zone of the TF (Figure 7c) experienced loss of strength and stiffness, with relevant damage level. Conversely, the panel zone of the IF (Figure 7d) was not affected by significant damage in terms of strength nor stiffness because the yield moment was not reached.

In the TF, the link element used for the simulation of the bar-slip phenomenon (Figure 7e) showed the first appearance of a degrading cyclic behavior.

As regards the friction device (Figure 7f), the seismic energy, which was absorbed by the panel zone and the beam-end plastic hinges in the TF, is now dissipated by the friction devices present in the IF. The hysteretic cycles of the FDD are wide and stable, having assumed that the cyclic performance of the device is not dependent on the cumulative displacement experienced.

By comparing Figure 7a2 and Figure 7b2, it is possible to observe that the connection with preloaded threaded bars and disk springs used in IF-TB undergoes lower maximum moment and larger rotation than those of the self-centering friction connection adopted in IF-FD. Consequently, reduced values of the overstrength factor could be used in the design of the column base. However, the lower yield moment leads to a weaker frame and, as already seen in Table 3, higher average MIDR values.

As already stated for the moment-rotation curves of the column bases depicted in Figure 7c2-f2, the only use of the FDD at the BCC in the IF does not prevent the formation of a plastic hinge. Conversely, the column bases behavior is elastic when the threaded bars or the self-centering friction

Table 3. Average and CoV of maximum and residual interstory drift ratios of the four types of RC frames / Media e CoV di MIDR e RIDR dei quattro tipi di telai.

Story		TF	IF	IF-TB	IF-FD
		Maximum IDR			
1	Mean	2.72%	2.56%	3.17%	2.57%
	CoV	13.27%	18.14%	12.61%	13.86%
2	Mean	2.91%	2.84%	3.10%	2.65%
	CoV	11.16%	16.58%	17.04%	17.91%
		Residual IDR			
1	Mean	0.17%	0.47%	0.10%	0.09%
	CoV	77.99%	79.74%	86.60%	70.89%
2	Mean	0.14%	0.59%	0.24%	0.19%
	CoV	78.71%	78.15%	79.57%	76.96%

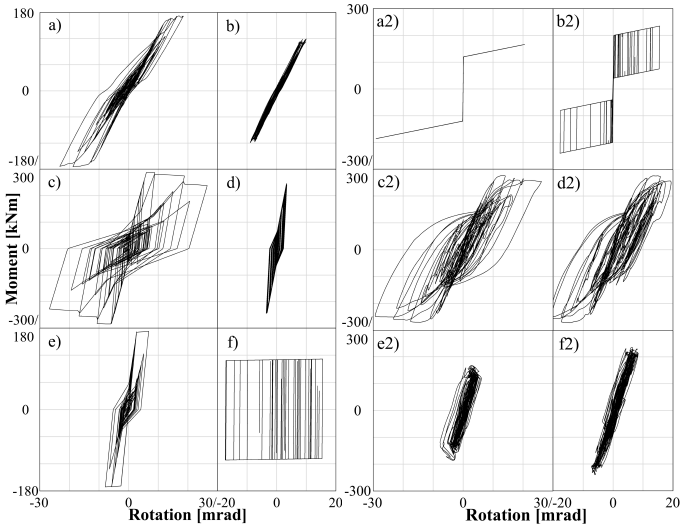

Figure 7. Moment-rotation curve of beam end section in TF (a), IF (b); beam-column joint shear deformation in TF (c), IF (d); bar-slip mechanism in TF (e); friction device in IF (f); the connection with preloaded threaded bars + disk springs of IF-TB (a2); the self-centering friction connection of IF-FD (b2); the column base in case of: TF (c2); IF (d2); IF-TB (e2); IF-FD (f2) / Diagramma momento-rotazione dell'estremità della trave TF (a), IF (b); deformazione a taglio del nodo trave-colonna in TF (c), IF (d); meccanismo di scorrimento della barra in TF (e); dispositivo ad attrito in IF (f); connessione con barre filettate pretensionate+molle a tazza in IF-TB (a2); connssione ad attrito ricentrante di IF-FD (b2); base della Colonna nel caso di: TF (c2); IF (d2); IF-TB (e2); IF-FD (f2).

connection are adopted in the IF-TB and IF-FD.

Finally, the Park & Ang damage Index (PAI) is calculated for assessing the different level of damage experienced by the four types of frames. In particular, an improved version of PAI is calculated for all the elements included in the above list, considering also left end of the first-story first-span beam:

$$PAI = \theta + E = \frac{\theta_{\max} - \theta_y}{\theta_u - \theta_y} + \frac{\beta}{M_y \theta_u} \int dE \qquad (8)$$

In Eq. (8), $\theta_{\max}$, θ_y, and θ_u are the maximum, the yielding, and the ultimate rotation experienced by the RC member, M_y is the yielding moment, $\int dE$ is the dissipated energy, and β is the model parameter, set equal to 0.15 for beams and columns and 0.25 for joint panels. As regards the joint panels, θ_y is obtained via MCFT, while θ_u is selected as suggested by De Risi, Ricci and Verderame (2017).

Table 4 reports θ_y, θ_u, M_y, average and CoV values of kinematic and hysteretic terms θ and E, and PAIs for the elements of the list above. The results obtained demonstrate that the damage of the RC members can be efficiently prevented or at least limited by the adoption of such innovative systems. In particular, with regard to beams, the small average PAI values for TF suggest that the beam-ends experience a small level of damage mostly due to the hysteretic behavior. On the other hand, average kinematic and hysteretic terms equal to 0 for beam-ends of IFs signify that they experience no plastic rotation and do not dissipate energy. For the column bases, large average and small CoV PAI values are obtained for TF, meaning that the bulk of central columns are near to the failure condition. By contrast, in the IF, the damage indexes of the columns are limited of about 20% compared to those of the TF, nevertheless their values overcome the limit of repairability, which is assumed equal to 0.4 (Park and Ang, 1985). The use of dissipative devices at the CFC proves to be efficient if the average PAI values of the column of IF-TB and IF-FD are considered (about 0.1 in both cases). As regards the panel joint, kinematic and hysteretic terms show the effectiveness of FDDs in the mitigation of structural damage. Conversely, in the TF, average PAI value near to 1 and low scatter suggest that the panel joint is near collapse in all the analyses, and it achieves failure condition in almost half of them. On the contrary, the panel joints

Table 4. Average and CoV values of Park & Ang damage Index (PAI), kinematic (θ) and hysteretic (E) terms for the left- and right-end of the first-story beams, column base, first-story internal joint, bar-slip mechanism of first-story beam / Medie e CoV dell'indice di danno PAI, (θ) e (E) per le estremità destra e sinistra delle travi del primo piano, della base del pilastro, del nodo interno del primo piano, del meccanismo di scorrimento delle barre della trave del primo piano.

Parameters			***θ***	***E***	***PAI***
Left end of the first-story first-span beam					
θ_y = 0.021 rad θ_u = 0.08 rad M_y^- = 169 kNm	TF	Avg	0.012	0.084	0.095
		CoV	182.98%	19.75%	36.07%
	IF/ IF-TB/ IF-FD	Avg	0	0	0
		CoV	-	-	-
Right end of the first-story second span beam					
θ_y = 0.021 rad θ_u = 0.08 rad M_y^+ = 174 kNm	TF	Avg	0.018	0.083	0.101
		CoV	218.39%	17.69%	50.75%
	IF/ IF-TB/ IF-FD	Avg	0	0	0
		CoV	-	-	-
Base section of the central column					
θ_y = 0.013 rad θ_u = 0.056 rad M_y = 278 kNm (for TF, IF, IF-TB) M_y = 326 kNm (for IF-FD)	TF	Avg	0.370	0.502	0.872
		CoV	26.72%	8.35%	13.42%
	IF	Avg	0.287	0.413	0.701
		CoV	38.59%	10.43%	19.50%
	IF-TB	Avg	0	0.118	0.118
		CoV	-	8.36%	8.36%
	IF-FD	Avg	0	0.080	0.080
		CoV	-	6.96%	6.96%
First-story internal joint					
θ_y = 0.006 rad θ_u = 0.065 rad M_y = 298 kNm (for TF) M_y = 406 kNm (for IF, IF-TB, IF-FD)	TF	Avg	0.331	0.651	0.982
		CoV	25.41%	7.21%	10.63%
	IF	Avg	0	0.179	0.179
		CoV	-	6.56%	6.56%
	IF-TB	Avg	0	0.178	0.178
		CoV	-	7.03%	7.03%
	IF-FD	Avg	0	0.184	0.184
		CoV	-	7.48%	7.48%
Bar-slip mechanism					
θ_y = 0.002 rad θ_u = 0.022 rad M_y = 169 kNm	TF	Avg	0.222	0.119	0.342
		CoV	63.07%	76.25%	65.67%

in innovative frames never reach the yield moment, leading to kinematic terms equal to 0, while hysteretic terms are drastically reduced if compared to that of TF. Finally, the bar-slip mechanism is characterized by a relatively small average PAI value which present high CoV and, thus, a small number of analyses are characterized by a bar-slip mechanism with PAI value above the limit of repairability.

6 CONCLUSIONS

The behavior of RC frames made with HSTCBs is investigated for analyzing their seismic response in presence of Friction Damper Devices (FDDs). Results obtained with the Traditional Frame (TF) prove that the most vulnerable elements are the joint panel zone, and the first story column base section, which both experience the greatest damaging in case of high intensity earthquakes and easily exceed the reparability threshold, up to the failure condition. On the contrary, the Innovative Frame (IF) endowed with FDDs only, exhibits beam end sections behave almost elastically and the panel zones experience negligible level of damage. However, column bases are still subjected to significant amount of damage. Also, the average RIDR obtained with the IF is much higher than that found in the TF and almost half of the analyses show RIDR values higher than the residual drift admissible, i.e. 0.5%. IF with Threaded Bars and disk springs (IF-TB) and IF with self-centering Friction Device (IF-FD) are characterized by column base-sections which behave elastically; moreover, average RIDRs similar to those of the TF can be found. Nevertheless, IF-TB provides a higher average MIDR because of the limited dissipative capacity of the system. On the other hand, the IF-FD exhibits a completely undamaged behavior, prevents business disruption and ensures an average MIDR comparable to that of the TF, with smaller RIDR.

Nel presente lavoro è stata analizzata la risposta sismica di telai in c.a. realizzati mediante Travi PREM e dotati di Dispositivi Dissipativi ad Attrito (DDA). I risultati ottenuti mediante il Telaio Tradizionale (TT) dimostrano che gli elementi più vulnerabili sono il pannello di nodo e la sezione alla base dei pilastri del primo piano, che si danneggiano significativamente nel caso di terremoti distruttivi e superano facilmente la soglia di riparabilità, fino al raggiungimento della condizione di rottura. Al contrario, il Telaio Innovativo (TI) dotato soltanto di DDA, mostra che le estremità delle travi rimangono in fase elastica e i pannelli di nodo subiscono un livello di danno trascurabile. Tuttavia, le sezioni alla base dei pilastri subiscono ancora un elevato livello di danneggiamento. Inoltre, lo Spostamento d'Interpiano Residuo (SIR) medio ottenuto con il TI è molto più grande di quello ottenuto con il TT, e quasi la metà delle analisi mostrano valori di SIR maggiori di quello ammissibile, cioè 0.5%. Il TI con Barre Filettate e molle a tazza (TI-BF) e il TI con Dispositivo auto-ricentrante ad Attrito (TI-DA) sono caratterizzati da sezioni alla base dei pilastri che rimangono in campo elastico; inoltre, i SIR medi sono simili a quello del TT. Tuttavia, il TI-BF fornisce uno Spostamento d'Interpiano Massimo (SIM) medio maggiore a causa della limitata capacità dissipativa del sistema. Al contrario, il TI-DA mostra un comportamento totalmente privo di danni, evita l'interruzione d'uso della struttura e assicura un SIM medio simile a quello del TT, con un minore SIR.

REFERENCES

Colajanni, P., L. La Mendola, A. Monaco, and N. Spinella. 2016. Cyclic behavior of composite truss beam-to-RC column joints in MRFs. Key Engineering Materials 711:681-9. doi: 10.4028/www.scientific.net/KEM.711.681.

Colajanni, P., L. La Mendola, and A. Monaco. 2018a. Review of push-out and shear response of hybrid steel-trussed concrete beams. Buildings 8 (10): art. n. 134. doi: 10.3390/buildings8100134.

Colajanni, P., L. La Mendola, and A. Monaco. 2018b. Stress transfer and failure mechanisms in steel-concrete trussed beams: experimental investigation on slab-thick and full-thick beams. Construction and Building Materials 161 (1):267-81. doi: 10.1016/j.conbuildmat.2017.11.134.

Colajanni, P., L. La Mendola, A. Monaco, and S. Pagnotta. 2020. Dissipative connections of RC frames with prefabricated steel-trussed-concrete beams. *Ingegneria Sismica* 37 (1):51-63.

Colajanni, P., L. La Mendola, A. Monaco, and S. Pagnotta. 2021. Design of RC joints equipped with hybrid trussed beams and friction dampers. *Engineering Structures* 227:111442. doi: 10.1016/j.engstruct.2020.111442.

De Risi, M. T., P. Ricci, and G. M. Verderame. 2017. Modelling exterior unreinforced beam-column joints in seismic analysis of non-ductile RC frames. Earthquake Engineering and Structural Dynamics 46:899-923. doi: 10.1002/eqe.2835.

Ferrante Cavallaro, G., M. Latour, A. B. Francavilla, V. Piluso, and G. Rizzano. 2018. Standardised friction damper bolt assemblies time-related relaxation and installed tension variability. Journal of Constructional Steel Research 141:145-55. doi: 10.1016/j.jcsr.2017.10.029.

Latour, M., G. Rizzano, A. Santiago, and L. S. da Silva. 2019. Experimental response of a low-yielding, self-centering, rocking column base joint with friction dampers. *Soil Dynamics and Earthquake* Engineering 116:580-92. doi: 10.1016/j.soildyn.2018.10.011.

Lowes, L. N., and A. Altoontash. 2003. Modeling reinforced-concrete beam-column joints subjected to cyclic loading. Journal of Structural Engineering ASCE 129 (12):1686-97. doi: 10.1061/(ASCE)0733-9445(2003)129:12(1686).

Park, Y., and A. H. Ang. 1985. Mechanistic seismic damage model for reinforced concrete. Journal of Structural Engineering ASCE 111 (3):722-39. doi: 10.1061/(ASCE)0733-9445(1985)111:4(722).

Sivaselvan, M. V., and A. M. Reinhorn. 1999. Hysteretic models for cyclic behavior of deteriorating inelastic structures. MCEER-99-0018, Multidisciplinary Center for Earthquake Engineering Research, State University of New York at Buffalo, Buffalo, USA.